Eur. J. Mineral., 38, 531–543, 2026
https://doi.org/10.5194/ejm-38-531-2026

European Journal of Mineralogy
Open Access

Belmonteite, $CaMn_2(AsO_4)_2(H_2O)_5{\cdot}2H_2O$, a new arsenate mineral from the Mn ore deposits of the Graveglia Valley, eastern Liguria, Italy

Cristian Biagioni[1,2], **Jiří Sejkora**[3], **and Zdeněk Dolníček**[3]

[1]Dipartimento di Scienze della Terra, Università di Pisa, Via Santa Maria 53, 56126 Pisa, Italy
[2]Centro per l'Integrazione della Strumentazione scientifica dell'Università di Pisa (CISUP), Università di Pisa, Pisa, Italy
[3]Department of Mineralogy and Petrology, National Museum, Cirkusová 1740, 193 00 Prague 9, Czech Republic

Correspondence: Cristian Biagioni (cristian.biagioni@unipi.it)

Received: 7 June 2026 – Revised: 27 July 2026 – Accepted: 4 August 2026 – Published: 19 August 2026

Abstract. Belmonteite (IMA 2024-040), ideally $CaMn_2(AsO_4)_2(H_2O)_5{\cdot}2H_2O$, is a new arsenate mineral discovered in the Gambatesa mine, Graveglia Valley, Ne, Genoa Province, Liguria, Italy. It occurs as aggregates up to 0.5 mm in length, formed by thin tabular crystals, white in color, with a silky luster and white streak. A perfect {010} cleavage was observed. Associated minerals are tennantite-(Cu), calcite, and a still unidentified (Ca,Cu)-arsenate secondary phase. Calculated density is 2.677 g cm^{-3}. The empirical chemical formula of belmonteite is $(Ca_{0.86}Mn_{0.11}K_{0.01})_{\Sigma 0.98}(Mn_{1.90}Cu_{0.08}Al_{0.02})_{\Sigma 2.00}As_{2.01}O_8{\cdot}7H_2O$. Unit-cell parameters are $a = 8.8418(9)$, $b = 23.031(2)$, $c = 13.5270(14)$ Å, $V = 2754.6(5)$ Å^3, space group *Cmce*, $Z = 8$. The crystal structure of belmonteite was refined to $R_1 = 0.0385$ for 1195 unique reflections with $F > 4\sigma(F)$ and 129 refined parameters. It can be described as being formed by {010} layers of six-fold-coordinated Mn atoms decorated on both sides by (AsO_4) groups and Ca atoms. These heteropolyhedral layers are connected along *b* through H bonds. Belmonteite displays {010} layers topologically similar to those occurring in switzerite. The genesis of belmonteite is probably related to the circulation of As-rich oxidizing fluids within the Mn ore deposit exploited at the Gambatesa mine during its late-stage evolution. The name honors Donato Belmonte (born 1978) for his earlier contribution to the knowledge of the mineralogy of Liguria.

1 Introduction

Manganese ore deposits of eastern Liguria, hosted in Jurassic cherts belonging to the "Diaspri di Monte Alpe" Formation, are classic Italian mineralogical localities owing to the occurrence of both well-crystallized specimens, found mainly during the former mining activity, and rare mineral species, showing peculiar chemical compositions. Manganese-rich ore bodies were affected by prehnite–pumpellyite facies metamorphism ($P = 0.25 \pm 0.05$ GPa, $T = 275 \pm 25$ °C) and by a hydrothermal remobilization along fractures under decreasing T–P conditions, leading to the genesis of polyphase mineral assemblages (Cabella et al., 1991, 1998). In particular, the late-stage hydrothermal fluids were able to further concentrate dispersed elements such as As, V, and Te, promoting the crystallization of minerals with unusual crystal chemical features, e.g., tiragalloite (Gramaccioli et al., 1980) and medaite (Gramaccioli et al., 1982). These two species were among the first hints of the interesting mineral assemblages of the Mn ore deposits of eastern Liguria.

Whereas Te minerals are very rare, having been discovered in very low amounts (e.g., Bindi et al., 2013; Carbone et al., 2013; Castellaro et al., 2021), V and As minerals are more widespread. At the beginning of the 1980s, Antofilli et al. (1983) cited the presence of conichalcite and sarkinite, along with the arsenato–trisilicate tiragalloite, and the vanadium oxy–salt minerals volborthite, medaite, and saneroite. Since then, a relatively large number of As and V miner-

als have been reported from the Mn ores of eastern Liguria (see, for instance, https://www.mindat.org/loc-21863.html, last access: 24 July 2026), and some of them were first described from these ore deposits.

Our re-examination of mineral specimens kept in the mineralogical collection of the Dipartimento di Scienze della Terra, dell'Ambiente e della Vita (DISTAV) of the University of Genoa yielded an unknown phase accompanied by a hand-written label bearing the wording "Ca-Mn arsenate?". The specimen was found by the mineral collector Corrado Balestra on the dumps of the Gambatesa mine at the beginning of the 1990s and at that time was given for analysis to Andrea Palenzona, who added it to his personal collection and later donated it to the DISTAV. Further investigations by X-ray diffraction revealed that the Ca–Mn arsenate kept in the DISTAV collection did not correspond to any known species. The new mineral, its name, and its symbol (Bmo) have been approved by the IMA Commission on New Minerals, Nomenclature and Classification (proposal IMA # 2024-040) as belmonteite. The name honors Donato Belmonte (born 1978) for his contributions to the mineralogy of Liguria. He co-authored the description of seven new mineral species from this region: cerchiaraite-(Fe) (Kampf et al., 2013), alpeite (Kampf et al., 2017), ramazzoite (Kampf et al., 2018), arsenmedaite (Biagioni et al., 2019), isselite (Biagioni et al., 2020), cortesognoite (Ma et al., 2023), and marioantofilliite (Biagioni et al., 2025). Moreover, he participated in the study of the 1*M* polytype of lavinskyite (Kolitsch et al., 2018). He also gave original insights into the understanding of the mineral associations in rodingitic and metarodingitic rocks from the Ligurian Alps and Apennines (e.g., Belmonte et al., 2018; Haws et al., 2021; Xiong et al., 2024; Xiong et al., 2026).

Type material for belmonteite is deposited in the mineralogical collection of the Dipartimento di Scienze della Terra dell'Ambiente e della Vita (DISTAV) of the University of Genoa, under catalogue number MO720. The sample used for single-crystal X-ray diffraction studies is kept in the mineralogical collection of the Museo di Storia Naturale, University of Pisa, Via Roma 79, Calci (Pisa, Italy), under catalogue number 20076.

2 Occurrence and physical properties

Belmonteite was discovered in a sample collected in the dumps of the Gambatesa mine (latitude 44°21′34″ N, longitude 9°26′59″ E), Graveglia Valley, Ne, Genoa Province, Liguria, Italy. This mine exploited braunite ore bodies hosted near the base of an Upper Jurassic metachert sequence ("Diaspri di Monte Alpe" Formation) which overlays Middle Jurassic ophiolites of the northern Apennine (Cabella et al., 1998). The Gambatesa mine is the type locality for six additional mineral species: cavoite (Basso et al., 2003), gravegliaite (Basso et al., 1991), poppiite (Brigatti et al., 2006), reppiaite (Basso et al., 1992), saneroite (Lucchetti et al., 1981), and vanadomalayaite (Basso et al., 1994).

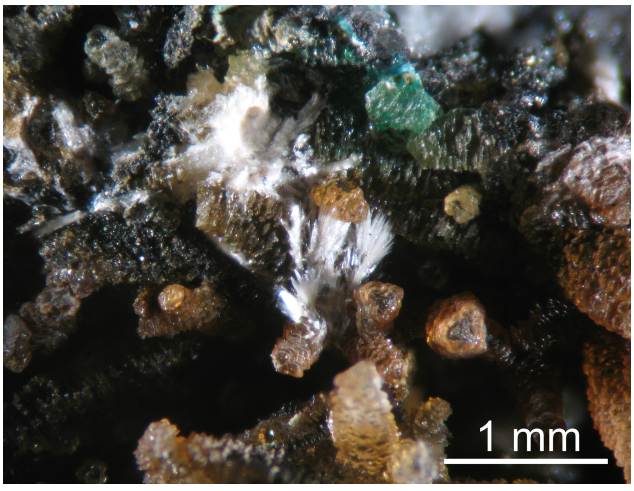

Figure 1. Belmonteite, aggregates of thin tabular crystals, white in color, with calcite; in the center, at the top, bluish spherulae of the mahnertite-like mineral can be observed. Gambatesa mine, Ne, Graveglia Valley, Genoa Province, Liguria, Italy. Holotype specimen, catalogue number MO720. Mineralogical collection of the Dipartimento di Scienze della Terra, dell'Ambiente e della Vita of the University of Genoa. Photo Cristian Biagioni.

Belmonteite occurs as aggregates, up to 0.5 mm in size, of thin tabular crystals, white in color, with a white streak and a silky luster (Fig. 1). The mineral is transparent, and it does not fluoresce under short- and long-wavelength UV radiation. Belmonteite is brittle, and it shows a perfect {010} cleavage. Calculated density is 2.677 g cm^{-3} based on the empirical formula and unit-cell parameters measured using single-crystal X-ray diffraction. Owing to the very low amount of material available for the mineral characterization, optical properties were not measured. The mean refraction index of belmonteite is 1.578, as obtained from the Gladstone–Dale relationship (Mandarino, 1979, 1981).

Belmonteite occurs in vugs of a carbonate vein, in association with tennantite-(Cu), calcite, and a still unidentified Cu secondary phase. Qualitative EDS chemical analysis of this latter phase revealed the occurrence of Ca, Cu, As, Cl, and minor S, whereas its X-ray powder diffraction pattern is similar but not identical to that of mahnertite, ideally $(Na,Ca,K)Cu_3(AsO_4)_2Cl(H_2O)_3{\cdot}2H_2O$. In the same mineral assemblage, luzonite has been identified through X-ray powder diffraction and EDS analysis (Donato Belmonte, personal communication, 2026).

The genesis of belmonteite is probably related to the circulation of As-rich oxidizing fluids during the late-stage evolution of the Mn ore deposit formerly exploited at the Gambatesa mine.

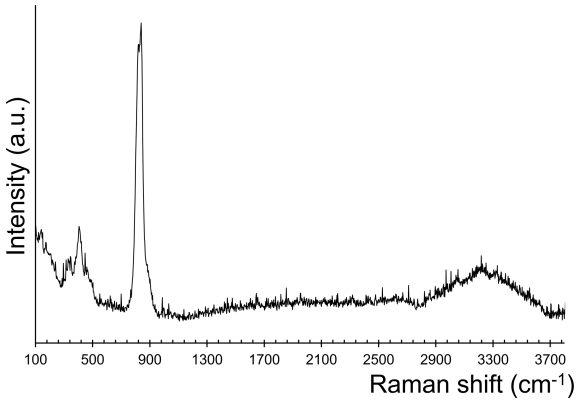

Figure 2. Raman spectrum of belmonteite in the full range (100–4000 cm^{-1}).

3 Raman spectroscopy

The Raman spectrum of belmonteite was collected in the range of 100–4000 cm^{-1} on an unpolished grain in nearly backscattered geometry using a Horiba Jobin-Yvon XploRA Plus apparatus, equipped with a motorized x–y stage and an Olympus BX41 microscope with a 50× objective. The Raman signal was excited by an unpolarized green diode-pumped solid-state laser ($\lambda = 532$ nm) and detected by a CCD detector. The minimum lateral and depth resolution was set to a few µm. The system was calibrated using the 520.6 cm^{-1} Raman band of silicon before each experimental session. Spectra were collected through multiple acquisitions (3) with single counting times of 30 s and laser power of 2.5 mW. Backscattered radiation was analyzed with a 1200 gr mm^{-1} grating monochromator. The possible thermal damage of the measured points was excluded by visual inspection of the excited surface after measurement by observation of possible decay of the spectral features in the start of the excitation and by checking for thermal downshift of Raman lines. The Raman spectrum of belmonteite is shown in Fig. 2.

The region between 100 and 1200 cm^{-1} is characterized by a strong band at 839 cm^{-1}, with shoulders at 815 and 891 cm^{-1}. These bands can be attributed to the ν_1 and ν_3 stretching modes of AsO_4 groups. Weaker bands at 336, 406, and 467 cm^{-1} can be interpreted as being due to the ν_4 and ν_2 bending modes of AsO_4 groups (e.g., Kloprogge, 2021). This band interpretation is in keeping with those proposed for other manganese arsenates (e.g., Frost and Weier, 2006; Kampf et al., 2016; Koshlyakova et al., 2026). In the O–H-stretching region (Fig. 2), a weak band and a broad band occur at 2900–3700 cm^{-1}, in agreement with the occurrence of H_2O groups in belmonteite (see below).

4 Chemical data

Quantitative chemical analyses of belmonteite were carried out using a Cameca SX 100 electron microprobe (WDS mode, 15 kV, 10 nA, 10 µm beam diameter) on a polished crystal surface at the National Museum, Prague, Czech Republic. The results (average of eight spot analyses) are given in Table 1. Other sought elements (Na, P, Mg, Si, Pb, S, Cl, Sr, Fe, Zn, F, N, V, and Cr) were below detection limits. Matrix correction by PAP algorithm (Pouchou and Pichoir, 1985) and automatic corrections of overlaps F–As and P–Ca were applied to the data. The occurrence of H_2O groups was confirmed by micro-Raman spectroscopy. Because insufficient pure material is available for a direct determination of H_2O, its amount has been calculated based upon the known stoichiometry from structure analysis. Belmonteite partly dehydrated in the electron microprobe chamber, and it is probable that it is also unstable under electron beam, as testified to by the high total after the addition of calculated H_2O (i.e., 116.74 wt %).

The empirical formula of belmonteite, on the basis of 15 O atoms per formula unit (apfu) and considering the results of the crystal structure study (see below), can be written as $(Ca_{0.86}Mn_{0.11}K_{0.01})_{\Sigma 0.98}(Mn_{1.90}Cu_{0.08}Al_{0.02})_{\Sigma 2.00}As_{2.01}O_8 \cdot 7H_2O$. The end-member formula is $CaMn_2(AsO_4)_2 \cdot 7H_2O$, corresponding to (in wt %) As_2O_5 41.49, CaO 10.12, MnO 25.61, H_2O 22.77, sum 100.00.

5 Crystallography

5.1 Powder X-ray diffraction

Powder X-ray diffraction data of belmonteite were collected using a Bruker D8 Venture single-crystal diffractometer equipped with a Photon III CCD area detector (microfocus Cu $K\alpha$ radiation) simulating a Gandolfi-like geometry (CISUP, University of Pisa, Italy). The observed X-ray diffraction lines are reported in Table 2, along with the calculated pattern based on the structural model discussed below. Unit-cell parameters were refined by the least-square program of Burnham (1962) as $a = 8.854(7)$, $b = 23.02(2)$, $c = 13.533(13)$ Å, $V = 2759(3)$ $Å^3$.

5.2 Single-crystal X-ray diffraction

Single-crystal X-ray diffraction intensity data were collected using a Bruker D8 Venture single-crystal diffractometer equipped with an air-cooled Photon III CCD detector and microfocus Mo $K\alpha$ radiation (CISUP, University of Pisa, Italy). The detector-to-crystal distance was 38 mm. Data were collected using ω and φ scan modes, in 0.5° slices, with an exposure time of 60 s per frame. A total of 1675 frames was collected. The frames were integrated with the Bruker *SAINT* software package using a narrow-frame algorithm. Data were corrected for Lorentz-polarization, ab-

Table 1. Chemical data (in wt %) for belmonteite.

Constituent	Mean	Range ($n = 8$)	e.s.d. (σ)	Normalized	Reference material
As_2O_5	48.57	45.93–50.35	1.71	41.60	Clinoclase
Al_2O_3	0.22	0.08–0.69	0.20	0.19	Sanidine
CaO	10.12	9.75–10.40	0.22	8.67	Fluorapatite
MnO	29.94	28.85–30.35	0.49	25.65	Rhodonite
CuO	1.28	1.00–1.64	0.22	1.10	Chalcopyrite
K_2O	0.10	0.04–0.18	0.05	0.08	Sanidine
H_2O_{calc}	26.51			22.71	
Total	116.74			100.00	

Note that H_2O content was based on stoichiometry; e.s.d. denotes estimated standard deviation; n denotes number of spot analyses.

sorption, and background using the *Apex*4 software package (Bruker AXS Inc., 2022). Unit-cell parameters, refined on the basis of the XYZ centroid of 5787 reflections above $20\sigma(I)$ with $4.645° < 2\theta < 56.44°$, are $a = 8.8418(9)$, $b = 23.031(2)$, $c = 13.5270(14)$ Å, $V = 2754.6(5)$ Å^3.

The statistical tests on the distribution of $|E|$ values ($|E^2 - 1| = 1.074$) suggest the occurrence of a center of symmetry. According to the systematic absences, the crystal structure of belmonteite was solved using *Shelxtl* (Sheldrick, 2015a) and refined in the space group *Cmce* using *Shelxl*-2018 (Sheldrick, 2015b). Neutral scattering curves, taken from the International Tables for Crystallography (Wilson, 1992), were used. Four independent cation sites, namely *As*(1), *As*(2), *Mn*(1), and *Ca*(2), and 12 anion positions were initially located, giving a structural model converging to $R_1 = 0.1298$. Two of the anion sites are mutually exclusive and are related to the positional disorder of the *As*(2)-centered tetrahedron. Consequently, their site occupancy was refined, restraining their sum to 1. The refinement indicated that they are half-occupied, and, for this reason, their site occupancy was fixed. Moreover, the U_{eq} value of the *Ca*(2) site was relatively large, and the site occupancy at this site was also refined, pointing to a partial occupancy of this position. After the modeling of the anisotropic displacement parameters for the cation positions, the examination of the difference Fourier maps revealed the occurrence of two other maxima represented by a split-O position. In the final stages of the refinement, the splitting of some O positions was further modeled, and their site occupancy was fixed to 0.5. After several cycles of anisotropic refinement for both cations and anions, the conventional R_1 factor converged to 0.0385 for 1195 unique reflections with $F > 4\sigma(F)$ and 129 refined parameters.

Details of the data collection and crystal structure refinement are given in Table 3. Atom coordinates and isotropic or equivalent isotropic displacement parameters are reported in Table 4, whereas Table 5 gives selected bond distances. Bond-valence calculation, shown in Table 6, was performed using the bond parameters of Gagné and Hawthorne (2015).

6 Crystal structure

6.1 General structural features

The crystal structure of belmonteite (Fig. 3) is formed by {010} layers of six-fold-coordinated Mn atoms, decorated on both sides by (AsO_4) groups and Ca atoms. These heteropolyhedral layers are connected along *b* through H bonds (Fig. 3a). Manganese-centered *Mn*(1) octahedra form zig-zag ribbons through edge-sharing, running along *a*, and are connected to adjacent ribbons along *c* through corner-sharing (Fig. 3b). Along every ribbon, to avoid too-short O···O distances (∼ 1.96 Å), two possible, mutually exclusive O positions are statistically occupied, i.e., O(7a) and O(7b). This disorder is related to the orientation of one of the (AsO_4) groups, i.e., that centered by *As*(2) (Fig. 4). Moreover, the *Ca*(2) site is only half-occupied. Such a disorder also affects the O(8), Ow(10), Ow(11), and Ow(12) sites. Specifically, Ow(12) is split into two positions, Ow(12a) and Ow(12b). The former is too close to *Ca*(2) and is occupied only when *Ca*(2) is empty; on the other hand, when *Ca*(2) is occupied, Ow(12b) occurs. Both Ow(12a) and Ow(9) are free H_2O groups as they are not bonded to any cation and are involved in H bonds.

6.2 Cation coordination

Arsenic atoms are hosted at the *As*(1) and *As*(2) sites and show the typical tetrahedral coordination of As^{5+}. At the *As*(1) site, As is coordinated by O atoms at one O(6) site, two O(4) sites, and one O(1) site, with average bond distance of 1.674 Å, slightly shorter than the value given by Majzlan et al. (2014), i.e., 1.685 Å. Its bond-valence sum is 5.18 valence units (v.u.). The *As*(2) tetrahedron suffers some rotational disorder, and two ordered configurations are possible (Fig. 4), related to the occupancy of the O(8) and the mutually exclusive O(7a) and O(7b) sites. The average bond distance is 1.683 Å, and the corresponding bond-valence sum is 5.08 v.u.

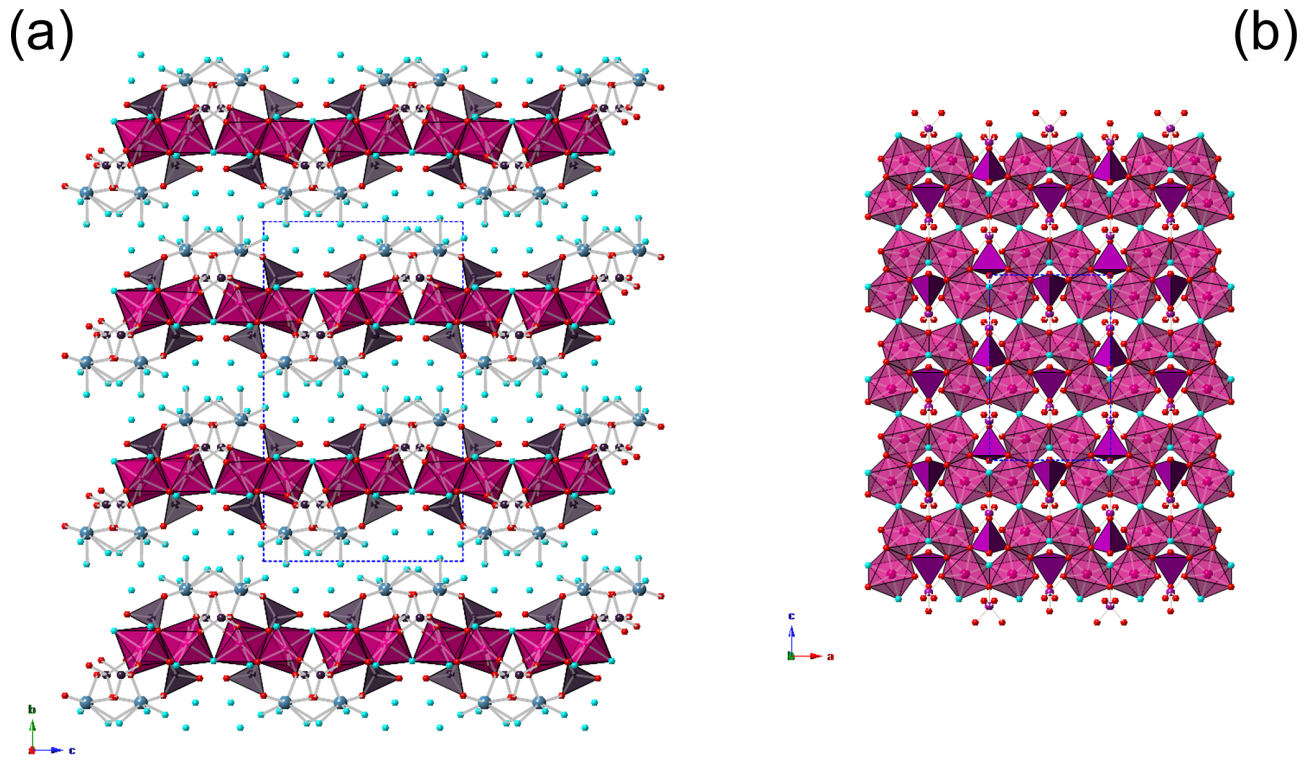

Figure 3. Crystal structure of belmonteite as seen down *a* **(a)**. In **(b)**, a {010} layer formed by Mn-centered *Mn*(1) sites and As-centered tetrahedra is shown. Symbols: magenta denotes *Mn*(1) octahedra, and violet denotes *As*(1) tetrahedra. Circles: red denotes O sites, light blue denotes H_2O groups, blue denotes *Ca*(2) sites, and violet denotes *As*(2) sites.

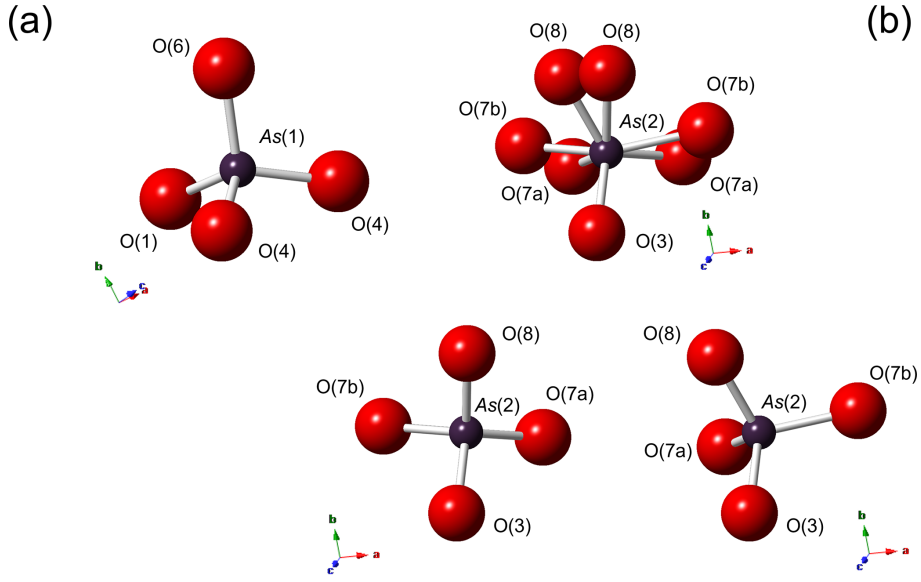

Figure 4. Coordination of As atoms hosted at *As*(1) **(a)** and *As*(2) **(b)**. Below, an ordered distribution of O atoms around *As*(2) is shown.

Manganese is hosted at the *Mn*(1) site, and it is octahedrally coordinated. Two possible configurations occur, involving O(7a) or O(7b) (Fig. 5) and related to the rotation of the *As*(2) tetrahedra. In the former case, the average ⟨Mn–O⟩ distance is 2.191 Å, with a bond-valence sum of 2.09 v.u.; in the latter case, an average distance of 2.211 Å is observed, with a bond-valence sum of 1.98 v.u. Both configurations agree with the occurrence of Mn^{2+} at the *Mn*(1) site. In Table 6, the average configuration involving half-occupied

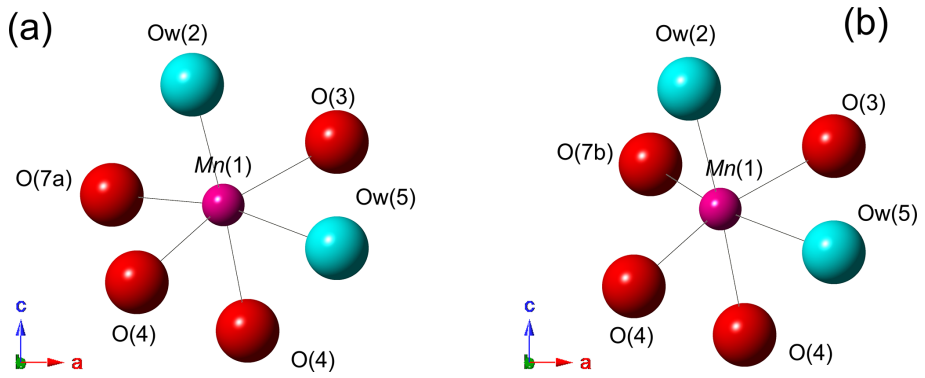

Figure 5. Coordination of Mn atoms hosted at *Mn*(1) in accordance with the occupancy of the O(7a) **(a)** and O(7b) **(b)** sites.

O(7a) and O(7b) is considered, resulting in an average bond-valence sum of 2.04 v.u.

Calcium cations are hosted at the *Ca*(2) site. In its first coordination sphere ($d < 3.0$ Å), there are 10 O sites, but some of them cannot be fully occupied, i.e., O(8), Ow(10), Ow(11), and Ow(12a)/Ow(12b). In particular, the occupancy of the *Ca*(2) site is mutually exclusive with Ow(12a), which is too close to *Ca*(2), i.e., 1.139(12) Å. In an ordered model, Ca atoms at the *Ca*(2) site show a distorted octahedral coordination. Oxygen atoms at O(6), O(7b), and Ow(12b) always belong to the coordination sphere of *Ca*(2), whereas different configurations for O(8), Ow(10), and Ow(11) can be hypothesized. There are eight different combinations (Table 7), corresponding to average bond distances in the range of 2.33–2.54 Å and bond-valence sums ranging from 1.56 to 2.18 v.u. Considering the partial occupancy of some ligand positions, the weighted bond-valence sum at the *Ca*(2) site is 1.87 v.u. (Table 6), agreeing with occurrence of Ca^{2+}, and the average bond distance is 2.433 Å, to be compared with the value of 2.371 Å proposed by Hawthorne and Gagné (2024) for six-fold-coordinated Ca^{2+} ion. However, as will be discussed below, an ordered model can be proposed, and, even if some of the eight possible configurations reported in Table 7 give physically reasonable average distances and bond-valence sums, only one configuration seems more probable.

6.3 Anion coordination and possible H bonds

In the crystal structure of belmonteite, 12 O sites have been located, with 2 of them being split. The examination of bond-valence sums at the anion positions (Table 6) allows us to identify three groups of anions, i.e., (i) anions with bond-valence sums close to 2 v.u., corresponding to O^{2-} anions; (ii) anions with bond-valence sums ranging from ∼ 1.3 and 1.7 v.u., probably corresponding to O^{2-} anions acting as acceptors in H bonds; and (iii) anions with bond-valence sums less than 0.6 v.u., represented by H_2O groups.

An accurate description of the H-bond system in belmonteite cannot be given, owing to the disorder affecting several atom positions and the missing location of H atoms. However, some features can be described. Oxygen atoms at the O(1) site are the acceptors of three H bonds from two H_2O groups hosted at Ow(2) and one hosted at Ow(9). Considering a bond strength of 0.25 v.u. for each H bond, three of them give 0.75 v.u., which allows the bond-valence sum at O(1) to be increased up to ∼ 2 v.u.

Oxygen atoms at the O(6) site have bond-valence sums lower than the ideal one, but they are acceptors of H bonds from Ow(10) and, when present, from Ow(12a). This could increase the bond-valence sum up to 2 v.u. Other O atoms with relatively low bond-valence sums are those at the O(7b) (affected by splitting) and O(8) sites. Atoms at this latter site may act as acceptors from Ow(11) (and also Ow(12a), when present), whereas O(7a) and O7(b) may be acceptors of H bonds from Ow(5) and Ow(12a), respectively. In this way, their bond-valence sums approach 2 v.u.

Other H bondings involving H_2O groups are more difficult to accurately describe. Ow(2) and Ow(5) act as donors to two O(1) sites and to O(7a) and Ow(9), respectively, whereas the actual H bonds involving Ow(9), Ow(10), Ow(11), and the pair Ow(12a)–Ow(12b) are affected by the local ordering. However, all of these positions are occupied by H_2O groups.

6.4 Structural disorder in belmonteite and the search for an ordered scheme

Notwithstanding the satisfactory R_1 value and the soundness of the crystal chemical features shown by belmonteite, the half-occupancy of the *Ca*(2) site and the rotational disorder of the *As*(2) site give reason for some further discussion. Indeed, one may think about a missing superstructure or wrong space group symmetry. With regards to the first point, the examination of the X-ray diffraction patterns did not reveal any hints of superstructure reflections, even if the diffraction quality and the small crystal size may prevent the collection of weak reflections.

The *C*-centered orthorhombic cell can be reduced to a *P*-monoclinic cell with unit-cell parameters $a = 12.3308(13)$, $b = 13.5241(14)$, $c = 8.8420(9)$ Å, $\beta = 110.986(4)°$, $V = 1376.7(2)$ Å^3, and space group $P2_1/c$, similar to those of the

Table 2. X-ray powder diffraction data (d in Å) for belmonteite.

I_{obs}	d_{obs}	d^*_{calc}	d^*_{calc}	I_{calc}	hkl
s	11.6	11.51	11.52	100	0 2 0
mw	8.9	8.77	8.77	22	0 2 1
mw	7.1	7.05	7.05	9	1 1 1
mw	5.37	5.33	5.33	7	1 3 1
w	5.24	5.24	5.23	2	1 1 2
–	–		4.421	2	2 0 0
–	–		4.199	4	0 2 3
–	–		3.957	2	1 1 3
–	–		3.559	6	1 3 3
–	–		3.550	5	0 4 3
mw	3.51	3.509	3.507	13	2 4 0
		3.497	3.497	14	1 5 2
vw	3.391	3.397	3.394	3	2 4 1
mw	3.049	3.047	3.044	14	2 2 3
mw	2.905	2.917	2.916	3	0 4 4
		2.900	2.898	13	2 6 0
vw	2.797	2.806	2.806	8	1 7 2
–	–		2.768	4	2 4 3
mw	2.684	2.688	2.686	3	2 0 4
		2.687	2.683	7	3 1 2
vw	2.622	2.618	2.616	2	2 2 4
vw	2.548	2.538	2.537	3	0 6 4
vw	2.446	2.224	2.449	2	0 4 5
vw	2.424	2.426	2.426	3	0 8 3
–			2.412	2	2 8 0
w	2.214	2.213	2.210	2	4 0 0
w	2.176	2.176	2.175	4	1 1 6
–	–		2.167	2	3 7 1
–	–		1.956	2	4 2 3
vw	1.915	1.919	1.919	2	0 12 0
vw	1.706	1.706	1.705	1	3 7 5
w	1.669	1.670	1.669	4	3 5 6
–	–		1.655	2	3 11 2
vw	1.605	1.606	1.604	2	5 5 2
w	1.574	1.574	1.573	2	3 7 6
vw	1.519	1.519	1.518	2	5 7 2

Note that I_{calc} and d_{calc} were obtained using PowderCell 2.4 (Kraus and Nolze, 1996) on the basis of the structural model of belmonteite given in Table 4. Only calculated reflections with $I_{calc} > 2$ (if not observed) are reported. The I_{obs} values were visually estimated: s – strong, mw – medium–weak; w – weak; vw – very weak. Values of d^*_{calc} were calculated on the basis of the unit-cell parameters refined using X-ray powder diffraction data.

Mn–phosphate switzerite, $Mn_3(PO_4)_2{\cdot}7H_2O$ (Zanazzi et al., 1986). However, the solution of the crystal structure of belmonteite in the monoclinic setting led to a worse R factor and to the appearance of several split-O positions. Other solutions were checked in different space groups belonging to the orthorhombic setting according to the systematic absences and the solutions proposed by *Shelxtl* (Sheldrick, 2015a), i.e., $Cmc2_1$, *Abm*2 (cell transformed according to [0 0 1| 1 0 0 | 0 1 0]) and *Aba*2 (transformation matrix [0 0 1 | 0 $\overline{1}$ 0 | 1 0 0]). The structural models solved and refined in the space groups $Cmc2_1$ and *Abm*2 still show the disorder associated with the As-centered tetrahedra (namely the *As*(2) site in the *Cmce* model). This disorder was removed in the structural model refined in the space group *Aba*2, but, in this case, the As-centered tetrahedron is distorted, with one of the O atoms possibly being split. Moreover, the ratio of the racemic twin component, 0.49(6), as well as some features like the occurrence of an O site close to one Ca site, like the pair *Ca*(2) / Ow(12a) in the model discussed above, still occurred. For this reason, the crystal structure of belmonteite has been proposed in the space group *Cmce*.

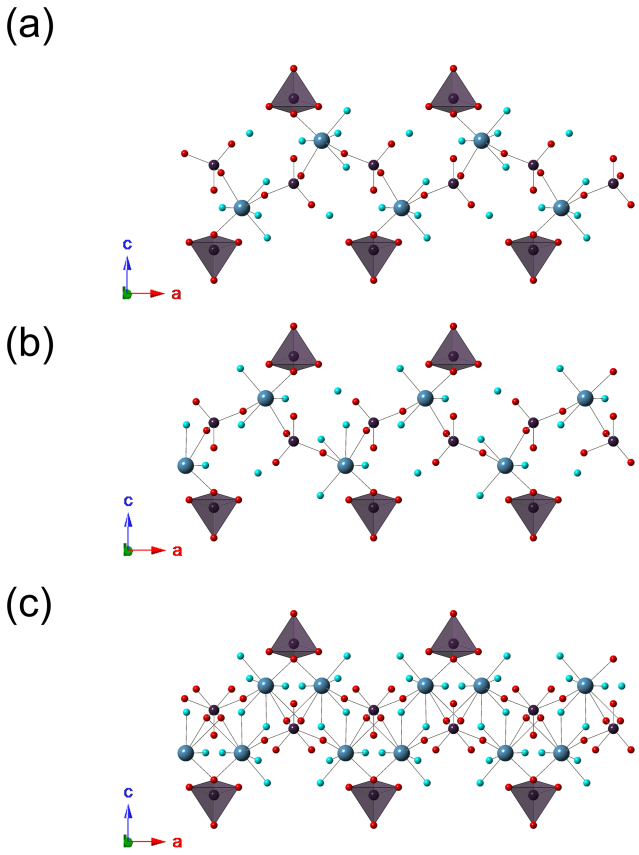

Figure 6. The [100] rods of *Ca*(2) polyhedra. In **(a)** and **(b)** are two possible ordered sequences, related to the different rotation of the *As*(2) tetrahedra. In **(c)**, the superposition of the **(a)** and **(b)** ordered sequences give rise to the observed disordered configuration. Same symbols as in Fig. 3.

The disorder observed in belmonteite is related to the rotation of the *As*(2) tetrahedron, which influences the coordination of both *Mn*(1) and *Ca*(2) sites. Figure 6 shows two possible ordered configurations of *Ca*(2) sites along a. The ordering has been obtained considering the two possible rotational configurations of the *As*(2) site and then avoiding too-short O···O contacts. Moreover, it has been considered to be the case that every O(6) atom belonging to the *As*(1) tetrahedra should be bonded to one *Ca*(2) atom. Indeed, if the O(6) were to be shared between two *Ca*(2) atoms, its bond-valence sum would be too high (2.31 v.u.), whereas it would be too

Table 3. Crystal and experimental data for belmonteite.

Crystal data	
Crystal size (mm)	$0.100 \times 0.050 \times 0.030$
Crystal system, space group	Orthorhombic, *Cmce*
a (Å)	8.8418(9)
b (Å)	23.031(2)
c (Å)	13.5270(14)
V (Å^3)	2754.6(5)
Z	8
Data collection and refinement	
Radiation, wavelength (Å)	Mo$K\alpha$, 0.71073
Temperature (K)	300(2)
$2\theta_{max}$ (°)	52.74
Measured reflections	29 235
Unique reflections	1507
Reflections with $F > 4\sigma$ (F)	1195
R_{int}	0.0954
$R\sigma$	0.0403
Range of h, k, l	$10 \le h \le 11, 28 \le k \le 28, 16 \le l \le 16$
R_1 $[F > 4\sigma$ $(F)]$	0.0385
R_1 (all data)	0.0525
wR_2 (on F^2)	0.1047
Goof	1.069
Number of least-squares parameters	129
Maximum and minimum residual peak (e Å^{-3})	0.78 [at 1.05 Å from *As*(2)] −0.80 [at 1.39 Å from *As*(1)]

Table 4. Sites, Wyckoff positions, site occupancy (s.o.), fractional atomic coordinates, and equivalent isotropic displacement parameters (in Å^2) for belmonteite.

Site	Wyckoff position	s.o.	x/a	y/b	z/c	U_{eq}
As(1)	8*f*	$As_{1.00}$	1/2	0.33374(3)	0.44028(5)	0.0164(2)
As(2)	8*f*	$As_{1.00}$	0	0.33395(3)	0.71216(5)	0.0181(2)
Mn(1)	16*i*	$Mn_{1.00}$	0.30360(9)	0.25738(3)	0.61452(6)	0.0201(2)
Ca(2)	16*i*	$Ca_{0.50}$	0.6757(2)	0.41659(9)	0.61231(16)	0.0228(5)
O(1)	8*f*	$O_{1.00}$	1/2	0.3443(2)	0.3172(4)	0.0215(11)
Ow(2)	8*e*	$O_{1.00}$	1/4	0.2045(2)	3/4	0.0257(12)
O(3)	8*f*	$O_{1.00}$	0	0.2919(2)	0.8146(4)	0.0258(12)
O(4)	16*i*	$O_{1.00}$	0.3456(5)	0.2961(2)	0.4726(3)	0.0400(11)
Ow(5)	8*f*	$O_{1.00}$	1/2	0.1925(2)	0.5658(4)	0.0354(14)
O(6)	8*f*	$O_{1.00}$	1/2	0.3960(2)	0.5027(5)	0.0393(16)
O(7a)	16*i*	$O_{0.50}$	0.1111(9)	0.3082(3)	0.6258(5)	0.0250(12)
O(7b)	16*i*	$O_{0.50}$	0.1832(9)	0.3351(3)	0.6648(7)	0.0250(12)
O(8)	16*i*	$O_{0.50}$	0.0449(8)	0.4015(3)	0.7439(6)	0.028(2)
Ow(9)	16*i*	$O_{0.50}$	0.466(4)	0.4153(4)	0.1615(8)	0.070(10)
Ow(10)	16*i*	$O_{0.50}$	0.4476(11)	0.5089(3)	0.6137(6)	0.046(3)
Ow(11)	16*i*	$O_{0.50}$	0.1720(11)	0.4767(4)	0.7204(8)	0.049(3)
Ow(12a)	16*i*	$O_{0.50}$	0.7760(14)	0.4422(4)	0.5823(9)	0.062(2)
Ow(12b)	16*i*	$O_{0.50}$	0.8340(13)	0.4511(4)	0.4902(9)	0.062(2)

Table 5. Selected bond distances (in Å) for belmonteite.

As(1)	–O(6)	1.664(5)	*As*(2)	–O(7a)	1.638(7) ×2
	–O(4)	1.675(4) ×2		–O(8)	1.662(7) ×2
	–O(1)	1.682(5)		–O(3)	1.690(5)
				–O(7b)	1.742(8) ×2
Mn(1)	–O(7a)	2.072(8)	*Ca*(2)	–O(6)	2.200(5)
	–O(3)	2.137(3)		–O(8)	2.290(8)
	–O(4)	2.149(4)		–Ow(12b)	2.306(12)
	–O(4)	2.155(4)		–O(7b)	2.362(8)
	–O(7b)	2.191(7)		–Ow(10)	2.389(8)
	–Ow(2)	2.251(3)		–Ow(11)	2.422(9)
	–Ow(5)	2.383(4)		–Ow(11)	2.653(10)
				–O(8)	2.777(8)
				–Ow(10)	2.931(9)

Table 6. Weighted bond-valence balance (in valence unit, v.u.) for belmonteite.

	As(1)	*As*(2)	*Mn*(1)	*Ca*(2)	Σ_{anions}
O(1)	1.27				1.27
Ow(2)			$^{2\times\rightarrow}$0.29		0.58
O(3)		1.24	$^{2\times\rightarrow}$0.39		2.02
O(4)	1.29$^{\downarrow\times2}$		0.38 0.37		2.04
Ow(5)			$^{2\times\rightarrow}$0.21		0.42
O(6)	1.33			0.49	1.82
O(7a)		1.44	0.46$^{1/2\times\downarrow}$		1.90
O(7b)		1.06	0.34 $^{1/2\times\downarrow}$	0.33	1.73
O(8)		1.34		0.40$^{1/2\times\downarrow}$ 0.12$^{1/2\times\downarrow}$	1.46^{a} 1.74^{b} 1.86^{c}
Ow(9)					0.00
Ow(10)				0.30 $^{1/2\times\downarrow}$ 0.08 $^{1/2\times\downarrow}$	0.08^{d} 0.30^{e} 0.38^{f}
Ow(11)				0.28 $^{1/2\times\downarrow}$ 0.16 $^{1/2\times\downarrow}$	0.16^{d} 0.28^{e} 0.44^{f}
Ow(12a)					0.00
Ow(12b)				0.38	0.38
$\Sigma_{cations}$	5.18	5.08	2.04	1.87	
Theor.	5.00	5.00	2.00	2.00	

Note that [a] means that O(8) is bonded to *As*(2) and *Ca*(2) through the long *Ca*(2)–O(8) distance of 2.78 Å; [b] O(8) bonded to *As*(2) and *Ca*(2) through the short Ca(2)–O(8) distance of 2.29 Å; [c] O(8) bonded to *As*(2) and two *Ca*(2); [d] Ow(10)/Ow(11) bonded to one *Ca*(2) at the longest Ca–Ow distance (2.93 and 2.65 Å, respectively); [e] Ow(10)/Ow(11) bonded to one *Ca*(2) at the shortest Ca–Ow distance (2.39 and 2.42 Å, respectively); and [f] Ow(10)/Ow(11) bonded to two *Ca*(2).

low if it were not to be bonded to any *Ca*(2) atom (1.33 v.u.). Considering these rules, the two ordered sequences, shown in Fig. 6a and b, can be obtained. In both cases, the bond distances around *Ca*(2) correspond to configuration no. 1 in Table 7. The disordered configuration observed in belmonteite (Fig. 6c) is the result of the superposition of the two configurations shown in Fig. 6a and b. The ordering seems to be unidirectional and does not significantly affect the overall topology of the {010} Mn layers that simply show a tilting of *Mn*(1) octahedra related to the orientation of *As*(2) tetrahedra. Consequently, every rod of *Ca*(2) polyhedra running along *a* may show a different orientation with respect to adjacent ones. This could result in the presence of streaks along a^* in the X-ray diffraction patterns, as observed in other species characterized by one-dimensional disorder, such as volaschioite and parnauite (Biagioni et al., 2011; Mills et al., 2013). Unfortunately, owing to the bad diffraction quality of belmonteite, reflection streaking was not observed.

6.5 Structural formula

On the basis of the crystal structure analysis, the structural formula of belmonteite can be written as $^{Ca(2)}(Ca\square)^{Mn(1)}Mn_2^{As(1)+As(2)}(AsO_4)_2(H_2O)_5{\cdot}2H_2O$ ($Z = 8$). Note that $^{Ca(2)}\square$ is not reported in the mineral formula as it is dictated by structural constraints.

Table 7. Different ligand configurations around the *Ca*(2) site (*d* in Å; bond-valence sum, BVS, in v.u.).

No. 1			No. 2			No. 3			No. 4		
Ca(2)	–O(6)	2.20	*Ca*(2)	–O(6)	2.20	*Ca*(2)	–O(6)	2.20	*Ca*(2)	–O(6)	2.20
	–O(8)	2.29		–O(8)	2.29		–O(8)	2.29		–O(8)	2.29
	–Ow(12b)	2.31		–Ow(12b)	2.31		–Ow(12b)	2.31		–Ow(12b)	2.31
	–O(7b)	2.36		–O(7b)	2.36		–O(7b)	2.36		–O(7b)	2.36
	–Ow(10)	2.39		–Ow(10)	2.39		–Ow(11)	2.65		–Ow(11)	2.42
	–Ow(11)	2.42		–Ow(11)	2.65		–Ow(10)	2.93		–Ow(10)	2.93
	average	2.33		average	2.37		average	2.46		average	2.42
	BVS	2.18		BVS	2.06		BVS	1.83		BVS	1.95
No. 5			**No. 6**			**No. 7**			**No. 8**		
Ca(2)	–O(6)	2.20	*Ca*(2)	–O(6)	2.20	*Ca*(2)	–O(6)	2.20	*Ca*(2)	–O(6)	2.20
	–Ow(12b)	2.31		–Ow(12b)	2.31		–Ow(12b)	2.31		–Ow(12b)	2.31
	–O(7b)	2.36		–O(7b)	2.36		–O(7b)	2.36		–O(7b)	2.36
	–Ow(10)	2.39		–Ow(10)	2.39		–Ow(11)	2.65		–Ow(11)	2.42
	–Ow(11)	2.42		–Ow(11)	2.65		–O(8)	2.78		–O(8)	2.78
	–O(8)	2.78		–O(8)	2.78		–Ow(10)	2.93		–Ow(10)	2.93
	average	2.41		average	2.45		average	2.54		average	2.50
	BVS	1.91		BVS	1.78		BVS	1.56		BVS	1.68

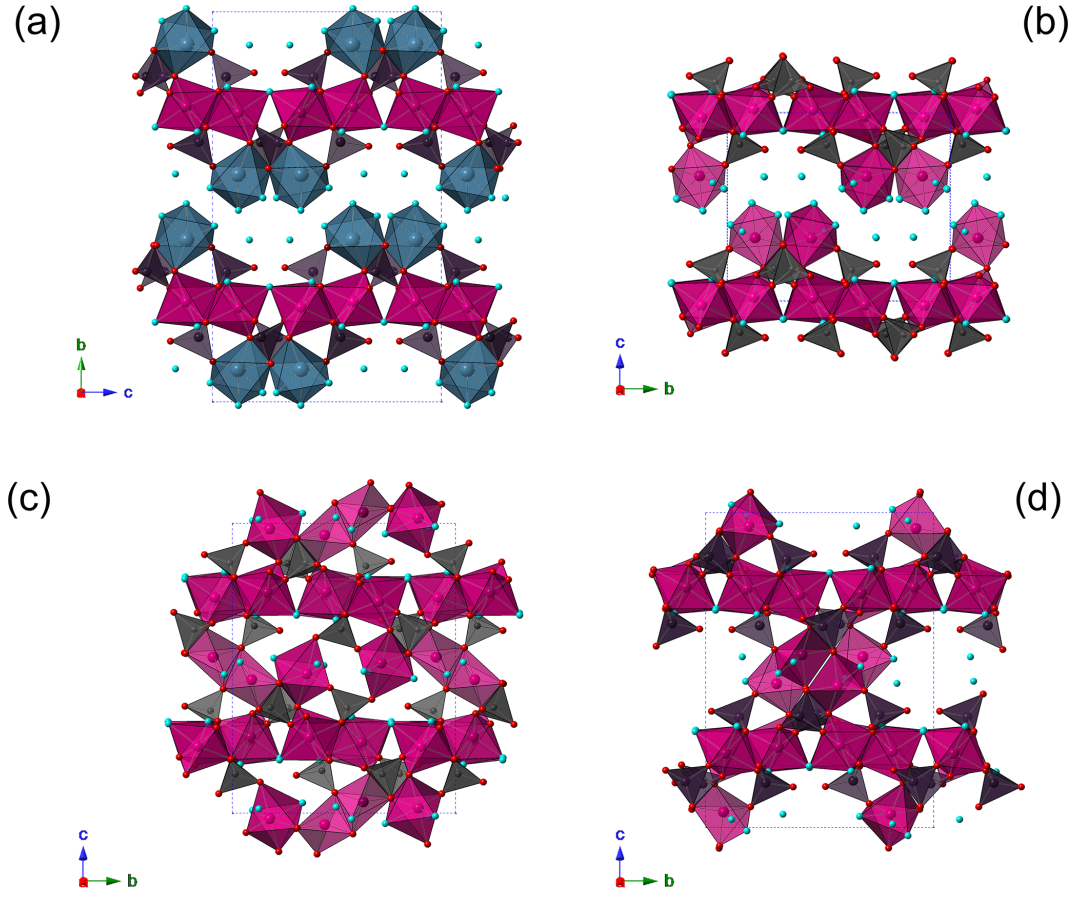

Figure 7. Comparison among the crystal structures of belmonteite **(a)**, switzerite **(b)**, metaswitzerite **(c)**, and castellaroite **(d)**. An ordered distribution of Ca and O atoms is shown for belmonteite.

Table 8. Minerals belonging to the CaO–MnO–As_2O_5–H_2O system.

Name	Chemical formula	a (Å)	b (Å)	c (Å)	α (°)	β (°)	γ (°)	s.g.	Ref.
Belmonteite	$CaMn_2(AsO_4)_2{\cdot}7H_2O$	8.84	23.03	13.53	90	90	90	*Cmce*	[1]
Brandtite	$Ca_2Mn(AsO_4)_2{\cdot}2H_2O$	5.88	12.96	5.68	90	108.0	90	$P2_1/c$	[2]
Fluckite	$CaMn(AsO_3OH)_2{\cdot}2H_2O$	8.46	7.61	6.97	82.2	98.2	95.9	$P\bar{1}$	[3]
Giftgrubeite	$CaMn_2Ca_2(AsO_4)_2(AsO_3OH)_2{\cdot}4H_2O$	18.50	9.48	9.99	90	96.8	90	$C2/c$	[4]
Parabrandtite	$Ca_2Mn(AsO_4)_2{\cdot}2H_2O$	5.89	7.03	5.64	96.8	109.3	108.5	$P1$ or $P\bar{1}$	[5]
Villyaellenite	$MnMn_2Ca_2(AsO_4)(AsO_3OH)_2{\cdot}4H_2O$	18.55	9.52	10.01	90	97.0	90	$C2/c$	[6]
Wallkilldellite	$Ca_2Mn_3(AsO_4)_2(OH)_4{\cdot}9H_2O$	6.51	6.51	23.49	90	90	120	$P6_3/mmc$, $P6_3mc$ or $P\bar{6}2c$	[7]

Note that s.g. denotes space group. [1] This work; [2] Herwig and Hawthorne (2006); [3] Catti et al. (1980); [4] Meisser et al. (2019); [5] Dunn et al. (1987); [6] Sarp (1984); [7] Dunn and Peacor (1983).

7 Relation to other species

Belmonteite is a new member of the quaternary chemical system CaO–MnO–As_2O_5–H_2O (Table 8). Its Ca/Mn atomic ratio is the same as those in manganlotharmeyerite, but this latter species is a Mn^{3+} phase belonging to the tsumcorite group (Brugger et al., 2002).

The {010} Mn layer occurring in belmonteite has the composition $Mn_4O_{10}(H_2O)_4$ ($Z = 4$) and a and c translations of 8.84 and 13.53 Å, respectively. This layer is topologically similar to those occurring in switzerite, ideally $Mn_3(PO_4)_2{\cdot}7H_2O$, and its dehydration product metaswitzerite, $Mn_3(PO_4)_2{\cdot}4H_2O$ (Fig. 7). The in-plane translations are 8.53 and 13.17 Å for the former and 8.50 and 13.17 Å for the latter (Fanfani and Zanazzi, 1979; Zanazzi et al., 1986). As discussed by Kampf et al. (2016), this kind of layer occurs in other phosphate minerals, and the first arsenate one characterized by this structural feature was castellaroite, $Mn_3(AsO_4)_2{\cdot}4.5H_2O$ (Kampf et al., 2016) (Fig. 7). A distorted but similar layer was also observed in picaite, $NaCa[AsO_3OH][AsO_2(OH)_2]$ (Kampf et al., 2019), even if the general topology of the crystal structure is different from that shown by belmonteite.

8 Conclusion

Belmonteite is further evidence of the most striking feature shown by arsenic minerals in metamorphic–hydrothermal environments – that is, the geochemical association between As and Mn, as stressed by Majzlan et al. (2014). Indeed, it is the sixth mineral species containing both As and Mn, having a type locality in the Mn ore deposits of eastern Liguria, after tiragalloite (Gramaccioli et al., 1980), coralloite (Callegari et al., 2012), castellaroite (Kampf et al., 2016), arsenmedaite (Biagioni et al., 2019), and monteneroite (Kampf et al., 2020).

The identification of belmonteite as a new mineral species has been possible after more than 30 years from its sampling. As described in the Introduction, a portion of the only known specimen was kept in the public mineral collection of the DISTAV, where it was easily accessible to researchers. In this way, publicly accessible mineral collections can be an important source of new mineral species because technological advancements make possible the crystal chemical investigation of mineral samples that could not be fully investigated with the analytical techniques available some decades ago. The discovery of belmonteite offers new information about the systematics of manganese arsenates and improves our knowledge of the complex mineral assemblages of the Mn ore deposits of eastern Liguria, a field of research that promises new, interesting findings, which may be hidden in some old mineral collection.

Data availability. The Crystallographic Information File of belmonteite is available in the Supplement.

Supplement. The supplement related to this article is available online at https://doi.org/10.5194/ejm-38-531-2026-supplement.

Author contributions. CB carried out the X-ray diffraction and Raman studies. JS and ZD conducted the electron microprobe analysis. CB wrote the paper, with inputs from the other authors.

Competing interests. At least one of the (co-)authors is a member of the editorial board of *European Journal of Mineralogy*. The peer-review process was guided by an independent editor, and the authors also have no other competing interests to declare.

Disclaimer. Publisher's note: Copernicus Publications remains neutral with regard to jurisdictional claims made in the text, published maps, institutional affiliations, or any other geographical representation in this paper. The authors bear the ultimate responsibility for providing appropriate place names. Views expressed in the text are those of the authors and do not necessarily reflect the views of the publisher.

Acknowledgements. The comments of Anthony R. Kampf and Igor V. Pekov improved the original paper.

Financial support. This research has been supported by the Ministry of Culture of the Czech Republic (long-term project DKRVO 2024-2028/1.II.c; National Museum, 00023272) through funding to Jiří Sejkora and Zdeněk Dolníček.

Review statement. This paper was edited by Cristiano Ferraris and reviewed by Anthony Kampf and Igor Pekov.

References

Antofilli, M., Borgo, E., and Palenzona, A.: I nostri minerali, Geologia e mineralogia in Liguria, Sagep, Genova, 295 pp., 1983.

Basso, R., Lucchetti, G., and Palenzona, A.: Gravegliaite, $MnSO_3{\cdot}3H_2O$, a new mineral from Val Graveglia (Northern Apennines, Italy), Z. Kristallogr., 197, 97–106, 1991.

Basso, R., Lucchetti, G., Zefiro, L., and Palenzona, A.: Reppiaite, $Mn_5(OH)_4(VO_4)_2$, a new mineral from Val Graveglia (Northern Apennines, Italy), Z. Kristallogr., 201, 223–234, 1992.

Basso, R., Lucchetti, G., Zefiro, L., and Palenzona, A.: Vanadomalayaite, $CaVOSiO_4$, a new mineral vanadium analog of titanite and malayaite, N. Jahr. Mineral. Monat., 1994, 489–498, 1994.

Basso, R., Lucchetti, G., Martinelli, A., and Palenzona, A.: Cavoite, CaV_3O_7, a new mineral from the Gambatesa mine, northern Apennines, Italy, Eur. J. Mineral., 15, 181–184, 2003.

Belmonte, D., Camarda, S., Sanguineti, G., Appiani, R., Bracco, R., and Zunino, F.: I minerali delle rodingiti in Liguria, Riv. Mineral. Ital., 42, 8–91, 2018.

Biagioni, C., Bonaccorsi, E., and Orlandi, P.: Volaschioite, $Fe_4^{3+}(SO_4)O_2(OH)_6{\cdot}2H_2O$, a new mineral species from Fornovolasco, Apuan Alps, Tuscany, Italy, Can. Mineral., 49, 605–614, 2011.

Biagioni, C., Belmonte, D., Carbone, C., Cabella, R., Zaccarini, F., and Balestra, C.: Arsenmedaite, $Mn_6^{2+}As^{5+}Si_5O_{18}(OH)$, the arsenic analogue of medaite, from the Molinello mine, Liguria, Italy: occurrence and crystal structure, Eur. J. Mineral., 31, 117–126, https://doi.org/10.1127/ejm/2018/0030-2792, 2019.

Biagioni, C., Belmonte, D., Carbone, C., Cabella, R., Demitri, N., Perchiazzi, N., Kampf, A. R., and Bosi, F.: Isselite, $Cu_6(SO_4)(OH)_{10}(H_2O)_4{\cdot}H_2O$, a new mineral species from Eastern Liguria, Italy, Mineral. Mag., 84, 653–661, 2020.

Biagioni, C., Sejkora, J., Perchiazzi, N., Mugnaioli, E., Mauro, D., Belmonte, D., Škoda, R., and Dolníček, Z.: Marioantofilliite, $[Cu_4Al_2(OH)_{12}](CO_3){\cdot}3H_2O$, a new member of the hydrotalcite supergroup from Liguria (Italy), Eur. J. Mineral., 37, 733–746, https://doi.org/10.5194/ejm-37-733-2025, 2025.

Bindi, L., Carbone, C., Belmonte, D., Cabella, R., and Bracco, R.: Weissite from Val Graveglia Mine, Liguria, Italy: occurrence, composition and determination of the crystal structure, Mineral. Mag., 77, 475–483, 2013.

Brigatti, M. F., Caprilli, E., and Marchesini, M.: Poppiite, the V^{3+} end-member of the pumpellyite group: Description and crystal structure, Am. Mineral., 91, 584–588, 2006.

Brugger, J., Krivovichev, S. V., Kolitsch, U., Meisser, N., Andrut, M., Ansermet, S., and Burns, P. C.: Description and crystal structure of manganlotharmeyerite, $Ca(Mn^{3+},\square,Mg)_2\{AsO_4,[AsO_2(OH)_2]\}_2(OH,H_2O)_2$, from the Starlera Mn deposit, Swiss Alps, and a redefinition of lotharmeyerite, Can. Mineral., 40, 1597–1608, 2002.

Bruker AXS Inc.: APEX4, Bruker Advanced X-ray Solutions, Madison, Wisconsin, USA, 2022.

Burnham, C. W.: Lattice constant refinement, Carnegie Institute Washington Yearbook, 61, 132–135, 1962.

Cabella, R., Gaggero, L., and Lucchetti, G.: Isothermal-isobaric mineral equilibria in braunite-, rhodonite-, johannsenite-, calcite-bearing assemblages from Northern Apennine metacherts (Italy), Lithos, 27, 149–154, 1991.

Cabella, R., Lucchetti, G., and Marescotti, P.: Mn-ores from Eastern Ligurian ophiolitic sequences ("Diaspri di Monte Alpe" Formation, Northern Apennines, Italy), Trends Mineral., 2, 1–17, 1998.

Callegari, A. M., Boiocchi, M., Ciriotti, M. E., and Balestra, C.: Coralloite, $Mn^{2+}Mn_2^{3+}(AsO_4)_2(OH)_2{\cdot}4H_2O$, a new mixed valence Mn hydrate arsenate: Crystal structure and relationships with bermanite and whitmoreite mineral groups, Am. Mineral., 97, 727–734, 2012.

Carbone, C., Basso, R., Cabella, R., Martinelli, A., Grice, J. D., and Lucchetti, G.: Mcalpineite from the Gambatesa mine, Italy, and redefinition of the species, Am. Mineral., 98, 1899–1905, 2013.

Castellaro, F., Passarino, G., Kampf, A. R., and Esposito, M.: Recenti ricerche mineralogiche nella sezione Cassagna delle miniere di manganese della Val Graveglia, Genova. Novità e conferme di mineralogia sistematica, Micro, 19, 34–60, 2021.

Catti, M., Chiari, G., and Ferraris, G.: Fluckite, $CaMn(HAsO_4)_2 \cdot 2H_2O$, a structure related to pseudo-polytypism to krautite $MnHAsO_4 \cdot H_2O$, Bull. Minéral., 103, 129–134, 1980.

Dunn, P. J. and Peacor, D. R.: Kittatinnyite and wallkilldellite, silicate/arsenate analogues containing calcium and manganese, from Franklin and Sterling Hill, New Jersey, Am. Mineral., 68, 1029–1032, 1983.

Dunn, P. J., Peacor, D. R., Su, S. C., Wicks, F. J., and Parker, F. J.: Parabrandtite, the manganese analogue of talmessite, from Sterling Hill, Ogdensburg, New Jersey, N. Jahr. Mineral. Abh., 157, 113–119, 1987.

Fanfani, L. and Zanazzi, P. F.: Switzerite: its chemical formula and crystal structure, Tschermaks Mineral. Petrogr. Mitt., 26, 255–269, 1979.

Frost, R. L. and Weier, M.: Raman and infrared spectroscopy of the manganese arsenate mineral allactite, Spectrochim. Acta A, 65, 623–627, 2006.

Gagné, O. C. and Hawthorne, F. C.: Comprehensive derivation of bond-valence parameters for ion pairs involving oxygen, Acta Crystallogr., B71, 562–578, 2015.

Gramaccioli, C. M., Griffin, W. L., and Mottana, A.: Tiragalloite, $Mn_4[AsSi_3O_{12}(OH)]$, a new mineral and the first example of arsenatotrisilicate, Am. Mineral., 65, 947–952, 1980.

Gramaccioli, C. M., Liborio, G., and Pilati, T.: Structure of medaite, $Mn_6[VSi_5O_{18}(OH)]$: the presence of a new kind of heteropolysilicate anion, Acta Crystallogr., B37, 1972–1978, 1982.

Haws, A. A., Starr, P. G., Dragovic, B., Scambelluri, M., Belmonte, D., Caddick, M. J., Broadwell, K. S., Ague, J. J., and Baxter, E. F.: Meta-rodingite dykes as recorders of subduction zone metamorphism and serpentinite dehydration: Voltri Ophiolite, Italy, Chem. Geol., 565, 120077, https://doi.org/10.1016/j.chemgeo.2021.120077, 2021.

Hawthorne, F. C. and Gagné, O. C.: New ion radii for oxides and oxysalts, fluorides, chlorides and nitrides, Acta Crystallogr., B80, 326–339, 2024.

Herwig, S. and Hawthorne, F. C.: The topology of hydrogen bonding in brandtite, collinsite and fairfieldite, Can. Mineral., 44, 1181–1196, 2006.

Kampf, A. R., Roberts, A. C., Venance, K. E., Carbone, C., Belmonte, D., Dunning, G. E., and Walstrom, R. E.: Cerchiaraite-(Fe) and cerchiaraite-(Al), two new barium cyclosilicate chlorides from Italy and California, USA, Mineral. Mag., 77, 69–80, 2013.

Kampf, A. R., Cámara, F., Ciriotti, M. E., Nash, B. P., Balestra, C., and Chiappino, L.: Castellaroite, $Mn_3^{2+}(AsO_4)_2{\cdot}4.5H_2O$, a new mineral from Italy related to metaswitzerite, Eur. J. Mineral., 28, 687–696, https://doi.org/10.1127/ejm/2016/0028-2535, 2016.

Kampf, A. R., Carbone, C., Belmonte, D., Nash, B. P., Chiappino, L., and Castellaro, F.: Alpeite, $Ca_4Mn_2^{3+}Al_2(Mn^{3+}Mg)(SiO_4)_2(Si_3O_{10})(V^{5+}O_4)(OH)_6$, a new ardennite-group mineral from Italy, Eur. J. Mineral., 29, 907–914, https://doi.org/10.1127/ejm/2017/0029-2636, 2017.

Kampf, A. R., Rossman, G. R., Ma, C., Belmonte, D., Biagioni, C., Castellaro, F., and Chiappino, L.: Ramazzoite, $[Mg_8Cu_{12}(PO_4)(CO_3)_4(OH)_{24}(H_2O)_{20}][(H_{0.33}SO_4)_3(H_2O)_{36}]$, the first mineral with a polyoxometalate cation, Eur. J. Mineral., 30, 827–834, https://doi.org/10.1127/ejm/2018/0030-2748, 2018.

Kampf, A. R., Nash, B. P., Celestian, A. J., Dini, M., and Molina Donoso, A. A.: Camanchacaite, chinchorroite, espadaite, magnesiofluckite, picaite and ríosecoite: six new hydrogen-arsenate minerals from the Torrecillas mine, Iquique Province, Chile, Mineral. Mag., 83, 655–671, 2019.

Kampf, A. R., Plášil, J., Nash, B. P., Ciriotti, M. E., Castellaro, F., and Chiappino, L.: Monteneroite, $Cu^{2+}Mn_2^{2+}(AsO_4)_2{\cdot}8H_2O$, a new vivianite-structure mineral with ordered cations from the Monte Nero mine, Liguria, Italy, Mineral. Mag., 84, 881–887, 2020.

Kloprogge, J. T.: Systematic Raman spectroscopic study of the isomorphy between the arsenate minerals roselite, wendwilsonite, zincroselite, brandtite, and rruffite, Appl. Spectrosc., 75, 846–856, 2021.

Kolitsch, U., Merlino, S., Belmonte, D., Carbone, C., Cabella, R., Lucchetti, G., and Ciriotti, M. E.: Lavinskyite-1*M*, $K(LiCu)Cu_6(Si_4O_{11})_2(OH)_4$, the monoclinic MDO equivalent of lavynskyite-2*O* (formerly lavinskyite), from the Cerchiara manganese mine, Liguria, Italy, Eur. J. Mineral., 30, 811–820, https://doi.org/10.1127/ejm/2018/0030-2731, 2018.

Koshlyakova, N. N., Pekov, I. V., Belakovskiy, D. I., Vigasina, M. F., Zubkova, N. V., Agakhanov, A. A., Britvin, S. N., Turchkova, A. G., Zhitova, E. S., Sidorov, E. G., and Pushcharovsky, D. Yu.: Manganobadalovite, $NaNaMn(MgFe^{3+})(AsO_4)_3$, a new alluaudite-group mineral from the Tolbachik Volcano, Kamchatka, Russia, Minerals, 16, 142, https://doi.org/10.3390/min16020142, 2026.

Kraus, W. and Nolze, G.: PowderCell – a program for the representation and manipulation of crystal structures and calculation of the resulting X-ray powder patterns, J. Appl. Crystallogr., 29, 301–303, 1996.

Lucchetti, G., Penco, A. M., and Rinaldi, R.: Saneroite, a new natural hydrated Mn-silicate, N. Jahr. Mineral. Monat., 1981, 161–168, 1981.

Ma, C., Carbone, C., and Belmonte, D.: Cortesognoite, $CaV_2Si_2O_7(OH)_2{\cdot}H_2O$, a new mineral from the Molinello manganese mine, Graveglia Valley, Italy, Crystals, 13, 1295, https://doi.org/10.3390/cryst13091295, 2023.

Majzlan, J., Drahota, P., and Filippi, M.: Parageneses and crystal chemistry of arsenic minerals, Rev. Mineral. Geochem., 79, 17–184, 2014.

Mandarino, J. A.: The Gladstone-Dale relationship. Part III. Some general applications, Can. Mineral., 17, 71–76, 1979.

Mandarino, J. A.: The Gladstone-Dale relationship. Part IV. The compatibility concept and some application, Can. Mineral., 19, 441–450, 1981.

Meisser, N., Plášil, J., Brunsperger, T., Lheur, C., and Škoda, R.: Giftgrubeite, $CaMn_2Ca_2(AsO_4)_2(AsO_3OH)_2{\cdot}4H_2O$, a new member of the hureaulite group from Sainte-Marie-aux-Mines, Haut-Rhin Department, Vosges, France, J. Geosci., 64, 73–80, 2019.

Mills, S. J., Kampf, A. R., McDonald, A. M., Bindi, L., Christy, A. G., Kolitsch, U., and Favreau, G.: The crystal structure of parnauite: a copper-arsenate-sulphate with translational disorder of structural rods, Eur. J. Mineral., 25, 693–704, https://doi.org/10.1127/0935-1221/2013/0025-2329, 2013.

Pouchou, J. L. and Pichoir, F.: "PAP" ($\varphi\rho$Z) procedure for improved quantitative microanalysis, 104–106, in: Microbeam Analysis, edited by: Armstrong, J. T., San Francisco Press, San Francisco, 1985.

Sarp, H.: Villyaellenite, $H_2(Mn,Ca)_5(AsO_4)_4{\cdot}4H_2O$, un noveau minéral de Saint-Marie aux Mines (France), Schweiz. Mineral. Petrogr. Mitt., 64, 323–328, 1984.

Sheldrick, G. M.: SHELXT – Integrated space-group and crystal-structure determination, Acta Crystallogr., A71, 3–8, 2015a.

Sheldrick, G. M.: Crystal structure refinement with SHELXL, Acta Crystallogr., C71, 3–8, 2015b.

Wilson, A. J. C. (Ed.): International Tables for Crystallography, Volume C: Mathematical, physical and chemical tables, Kluwer Academic, Dordrecht, NL, 1992.

Xiong, J.-W., Chen, Y.-X., Scambelluri, M., Qiao, X.-Y., Chen, Y., Huang, F., Belmonte, D., and Zhao, Z.-F.: Fluid-metasomatized rocks with extremely low δ^{26}Mg values in subducted oceanic lithosphere: implications for mantle Mg isotope heterogeneity and the origin of low- δ^{26}Mg magmas, Geochim. Cosmochim. Ac., 371, 111–125, 2024.

Xiong, J.-W., Chen, Y.-X., Qiao, X.-Y., Xu, J.-L., Li, X.-L., Scambelluri, M., Tsujimori, T., and Belmonte, D.: Light Fe isotopic fingerprints of serpentinite-derived fluids recorded by metasomatized mafic dikes in the subducted oceanic lithosphere, Earth Planet. Sci. Lett., 684, 120024, https://doi.org/10.1016/j.epsl.2026.120024, 2026.

Zanazzi, P. F., Leavens, P. B., and White Jr., J. S.: Crystal structure of switzerite, $Mn_3(PO_4)_2{\cdot}7H_2O$, and its relationship to metaswitzerite, $Mn_3(PO_4)_2{\cdot}4H_2O$, Am. Mineral., 71, 1224–1228, 1986.